

Near ultraviolet photonic integrated lasers based on silicon nitride

Anat Siddharth,¹ Thomas Wunderer,² Grigory Lihachev,¹ Andrey S. Voloshin,¹
Camille Haller,³ Rui Ning Wang,¹ Mark Teepe,² Zhihong Yang,² Junqiu Liu,¹ Johann
Riemensberger,^{1,*} Nicolas Grandjean,³ Noble Johnson,² and Tobias J. Kippenberg^{1,†}

¹*Laboratory of Photonics and Quantum Measurements,
Swiss Federal Institute of Technology Lausanne (EPFL), CH-1015 Lausanne, Switzerland*

²*Palo Alto Research Center, Palo Alto, CA 94304 USA*

³*Laboratory of Advanced Semiconductors for Photonics and Electronics,
Swiss Federal Institute of Technology Lausanne (EPFL), CH-1015 Lausanne, Switzerland*

Low phase noise lasers based on the combination of III-V semiconductors and silicon photonics are well established in the near infrared spectral regime [1]. Recent advances in the development of low-loss silicon nitride based photonic integrated resonators have allowed to outperform bulk external diode and fiber lasers in both phase noise [2, 3] and frequency agility [4] in the 1550 nm-telecommunication window. Here, we demonstrate for the first time a hybrid integrated laser composed of a gallium nitride (GaN) based laser diode and a silicon nitride photonic chip based microresonator operating at record low wavelengths as low as 410 nm in the near ultraviolet wavelength region suitable for addressing atomic transitions of atoms and ions used in atomic clocks, quantum computing, or for underwater LiDAR. Using self-injection locking to a high Q (0.4×10^6) photonic integrated microresonator we observe a phase noise reduction of the Fabry-Pérot laser at 461 nm by a factor greater than $10\times$, limited by the device quality factor and back-reflection.

Photonic integrated lasers that operate in the visible to ultraviolet (UV) spectral regime featuring narrow emission linewidth and low phase noise are required for the miniaturization of photonic systems. Applications for such systems range from quantum metrology and sensing [5] based on laser cooled neutral atoms and ions [6], precision atomic clocks [7], underwater laser range-finding [8], interferometric biophotonics [9], or visible spectroscopy [10, 11]. The wide band gap group III-Nitride semiconductor material family is ideally suited as active materials platform for next generation integrated photonics covering operation wavelengths in the UV and visible spectral regime. High power III-N laser sources (i.e. GaN and its alloys) are commercially available today and can be found in various products such as Blu-ray players, solid-state lighting devices or modern car headlamps. However, for neutral atom and ion based Quantum Information Science and Metrology applications, conventional III-N laser diodes cannot meet the requirements in terms of emission linewidth (i.e. phase noise) and longitudinal mode stability (i.e. drift) during operation. Instead, only external-cavity diode lasers using bulk precision optics

and gratings, which are frequency tuned via physical adjustment have achieved a suitable performance, exhibiting kHz linewidth [12]. Yet, the bulk nature of these laser systems, along with their weight, restrict applications in particular for space based applications. More compact blue lasers have been demonstrated based on crystalline resonators, yet these are not wafer scale compatible [13]. As a result, the development of single frequency III-N lasers has regained interest. These include Distributed Feedback Laser configurations for single frequency operation [14–18]. In contrast, silicon photonics-based lasers using heterogeneous and hybrid integration have enabled scalable, narrow linewidth and tunable lasers that are already employed at a commercial level in data center interconnects, typically operating in the 1550 nm telecommunication window [19]. Yet silicon’s bandgap limits access to shorter wavelength. Silicon nitride (Si_3N_4) is a good material to realize low loss integrated photonic circuits in the visible and ultraviolet wavelength spectral region, due to a wide bandgap of 4.9 eV, high refractive index 2.09 at 410 nm, CMOS-compatible fabrication, and established commercial foundry processes. Moreover major advances in nano-fabrication methods have enabled ultra-low propagation loss waveguides, reaching 1 dB/m [20]. Demonstrations using Si_3N_4 platform in the visible so far include blue laser based beam-forming [21], biophotonic probes [22], modulators [23] and visible photonic integrated lasers [24]. Laser cooling of atoms and ions (e.g. Ca^+ at 397 nm, Yb at 399 nm, Sr^+ at 420 nm and Sr at 461 nm, etc.) requires laser wavelength close to, or below 400 nm (cf. Figure 1f) with typically $\mathcal{O}(\text{mW})$ power levels. Integrating compact III-N laser gain elements with high-performance Si_3N_4 -based photonic circuits for single-frequency laser operation with narrow linewidth at wavelengths close to 400 nm has not yet been attained and the prospect for tunability and stable operation has not been explored in great detail so far. Here, the successful integration of an AlGaInN laser gain element coupled to a Si_3N_4 Photonic Integrated Circuit (PIC) platform featuring laser emission intrinsic linewidth of ~ 2.7 MHz is demonstrated with more than 10 dB frequency noise reduction via laser self injection locking. Such narrow linewidth laser sources, which via integration of AlN or PZT piezoelectric actuators can also be made frequency-agile, i.e. enable mode hop free scanning over $\mathcal{O}(10 \text{ GHz})$ with actuation bandwidth of

$\mathcal{O}(10\text{ MHz})$ as recently demonstrated [4], are ideal candidates for photonic integrated lasers for manipulating trapped-ion/atomic quantum systems or underwater coherent laser ranging.

RESULTS

III-N semiconductor based hybrid self-injection-locked lasers using Si_3N_4 -based integrated photonics. Figure 1 (a,b) depicts the experimental setup with a GaN-based Fabry-Pérot laser diode chip directly butt-coupled to a Si_3N_4 photonic chip. Custom AlGaInN near-UV laser diodes were fabricated on low-defect density native GaN substrates using Metal-Organic Vapor Phase Epitaxy (MOVPE). The epitaxial growth process was optimized towards high gain and low absorption losses within the laser heterostructure, balancing optical and electronic performance of the device. The active zone of the laser diode consists of multiple InGaIn quantum wells that are electrically pumped in a pn-junction architecture. The design was tailored for laser emission near 410 nm and is depicted in Fig. 1e. In this edge-type emitter configuration, transversal mode confinement is realized through the heterostructure layer stack where the active Multi-Quantum Well (MQW) zone is embedded in (Al)Ga(In)N waveguide and cladding layers featuring different Al-compositions. Lateral mode confinement is achieved via dry etching a narrow ridge into the p-side of the heterostructure and the creation of optical gain in the QWs right below the etched ridge. Lateral current confinement and the creation of localized gain is accomplished by ensuring electrical current injection exclusively through an opening in the electrical passivation layer on top of the laser ridge (cf. Figure 1e). The laser ridge had a width of nominally 1.5 microns and was etched to an optimized depth for laser operation of only one lateral mode. Laser mirror facets were realized via cleaving along the crystallographic m-plane of the III-N crystal. The laser resonator cavities were about 1 mm long. Optical facet coatings were applied to both the front and the rear facet for optimized laser characteristics. For full continuous wave (cw) operation individual laser die (LD) were mounted epi-side up onto thermal heat spreader sub-mounts and individually wire-bonded for both the n- and p-side. The LD-heat spreader sub-mount ensemble was then mounted into a standard TO-5 can. Special care was taken to allow for excellent laser facet exposure for optimal butt-coupling of the LD to the Si_3N_4 PIC chip. The laser diode showed a characteristic laser threshold of about 70 mA and can produce more than 100 mW of optical output power at a wavelength of 410 nm. The laser is mounted on a thermo-electric cooler for stabilizing its temperature and is operated at 21 degrees Celsius.

In addition, we also investigate longer wavelength lasers in this work, notably blue and green laser diodes (LDs) which were provided by Exalos AG [25]. The emis-

sion wavelength of the commercially available blue LD is between 457-464 nm with a threshold current around 18 mA. The green LD has emission wavelengths between 517-523 nm with threshold current around 38 mA.

The Si_3N_4 waveguides and microresonators are fabricated using a subtractive process [26] and have a uniform height and width of 50 nm and 600 nm, respectively. Stochiometric Si_3N_4 thin films are grown with low-pressure chemical vapor deposition (LPCVD) and etched in a fluorine chemistry. The waveguides and microresonators are defined by deep-ultraviolet stepper (248 nm) lithography. The cross section of the microresonators of the Si_3N_4 waveguide is depicted in Figure 1d. The waveguides are fully buried in SiO_2 cladding of 7 μm thickness. The bottom cladding is made of thermal oxide of 4 μm thickness whereas the top cladding is composed of 1 μm TEOS and 2 μm low temperature oxide (LTO). The entire device sits on a 230 μm -thick Si substrate. The radius of the microring resonator is 200 μm , corresponding to free spectral range of approximately 107.08 GHz. The thin Si_3N_4 supports the fundamental transverse electric (TE) mode at violet and blue wavelengths as shown in the inset with $\sim 14.5\%$ of E-field confined in Si_3N_4 core as shown in inset of Figure 1d. Development of a low-loss photonic platform in the blue and near ultraviolet spectral regime is challenging as Rayleigh scattering scales with λ^{-4} and material loss also increases as wavelengths approach the materials' bandgap. Figure 1b presents a cavity linewidth measurement of Si_3N_4 microresonator carried out at 461 nm, which reveals a loaded cavity linewidth $\kappa/2\pi = 2.33\text{ GHz}$ and an intrinsic linewidth $\kappa_0/2\pi = 1.69\text{ GHz}$, corresponding to an intrinsic quality factor of $\sim 0.4 \cdot 10^6$ (corresponding to a propagation loss of 3 dB/cm). The quality factor can be enhanced by designing waveguides with higher aspect-ratios and making a thinner Si_3N_4 core [27]. Such a design takes advantage of the lower material loss of the silica cladding and reduces the mode overlap with the sidewalls that minimizes sidewall scattering which is the primary contributor to loss in high-index-contrast planar waveguides. The Si_3N_4 waveguide is terminated at both ends with inverse tapers to facilitate laser diode to Si_3N_4 waveguide coupling and Si_3N_4 waveguide to lensed-fiber coupling. The butt-coupling scheme gives an overall insertion loss of $\sim 10.5\text{ dB}$ (diode-chip-lensed fiber), which we measure by comparing the free-space output power of the laser with the fiber-coupled power in the free-running laser regime. The insertion loss can be further reduced by using bi-layer silicon nitride edge couplers [28] that enhance fiber-to-chip light coupling in visible wavelength regime.

Figure 1c illustrates the laser self-injection locking principle. The key parameters that influence self-injection locking are the quality factor of the microresonator, Rayleigh backscattering and optical feedback phase (optical phase of back-scattered light). We tune the current of the laser diode and thus sweep the relative frequency between the laser and the resonator modes to

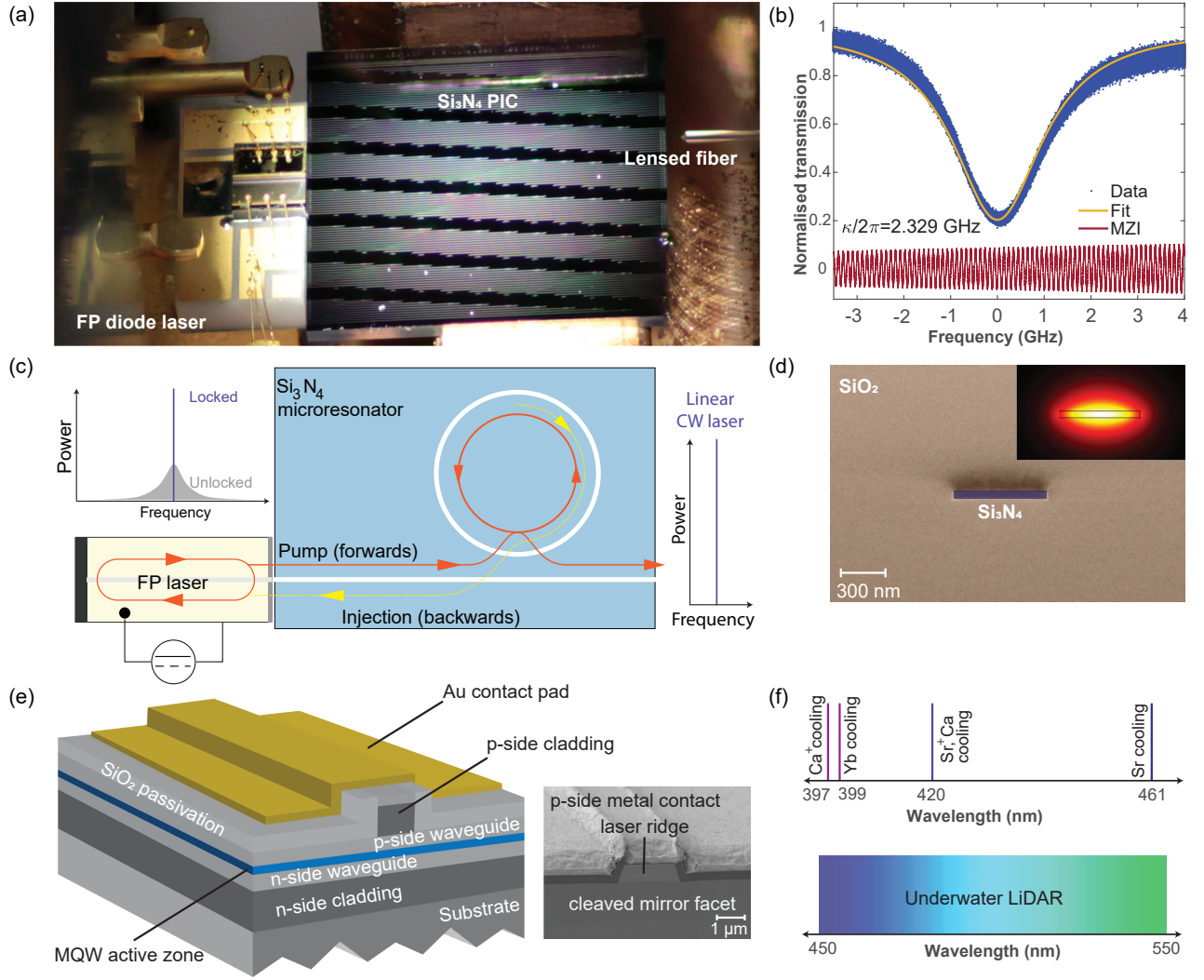


Figure 1. Schematic of the hybrid integrated laser system. (a) Photo of the experimental setup showing the Fabry-Pérot laser diode butt-coupled to the Si₃N₄ photonic chip and the output radiation is collected by a lensed fiber. (b) Measured transmission spectra of a mode using a tunable laser at 461 nm calibrated by a fiber-based Mach-Zehnder interferometer with free spectral range of 100.12 MHz. The measured loaded linewidth $\kappa/2\pi \approx 2.33$ GHz corresponding to loaded quality factor of $0.28 \cdot 10^6$. (c) Principle of laser linewidth narrowing via laser self-injection locking. (d) False-colored scanning electron microscope (SEM) image of the sample cross-section, showing a 50 nm thick Si₃N₄ buried in SiO₂ cladding of total thickness 6 μ m. The inset shows a finite-element method (FEM) simulation of the spatial distribution of the TE-mode electric-field amplitude at wavelength 461 nm. (e) Schematic showing the laser diode structure that emits laser light near-UV wavelengths (410 nm) with SEM image of the sample cross-section showing the laser ridge. (f) Relevant wavelength region covered by low noise III-N hybrid integrated photonic lasers and their different applications, including several ion transitions using for cooling.

attain self-injection locking. When the frequency of the light emitted from the laser diode is close to a high- Q resonance of the Si₃N₄ microresonator, laser self-injection locking takes place. The process occurs due to coupling of counter-propagating microresonator modes induced by Rayleigh back-scattering [29, 30]. This provides a frequency-selective narrowband optical feedback to the laser, leading to single-frequency operation and a reduction in the frequency noise of the laser [31].

Laser frequency noise measurements. Figure 2a illustrates the experimental scheme to measure the fre-

quency noise of the laser. The laser frequency noise is measured by performing heterodyne beat-note spectroscopy with a tunable external cavity diode laser (Topica DL Pro HP) with central wavelength at 461 nm as the reference. The electrical output of the photodiode is fed to a phase noise analyzer (Rhode & Schwarz FSW43). Figure 2b shows the heterodyne beat-note of the self-injection locked laser with the reference laser. The spectrum is fitted with the Voigt profile which provides the information about the Lorentzian and Gaussian contribution to the frequency noise of the laser. The Lorentzian

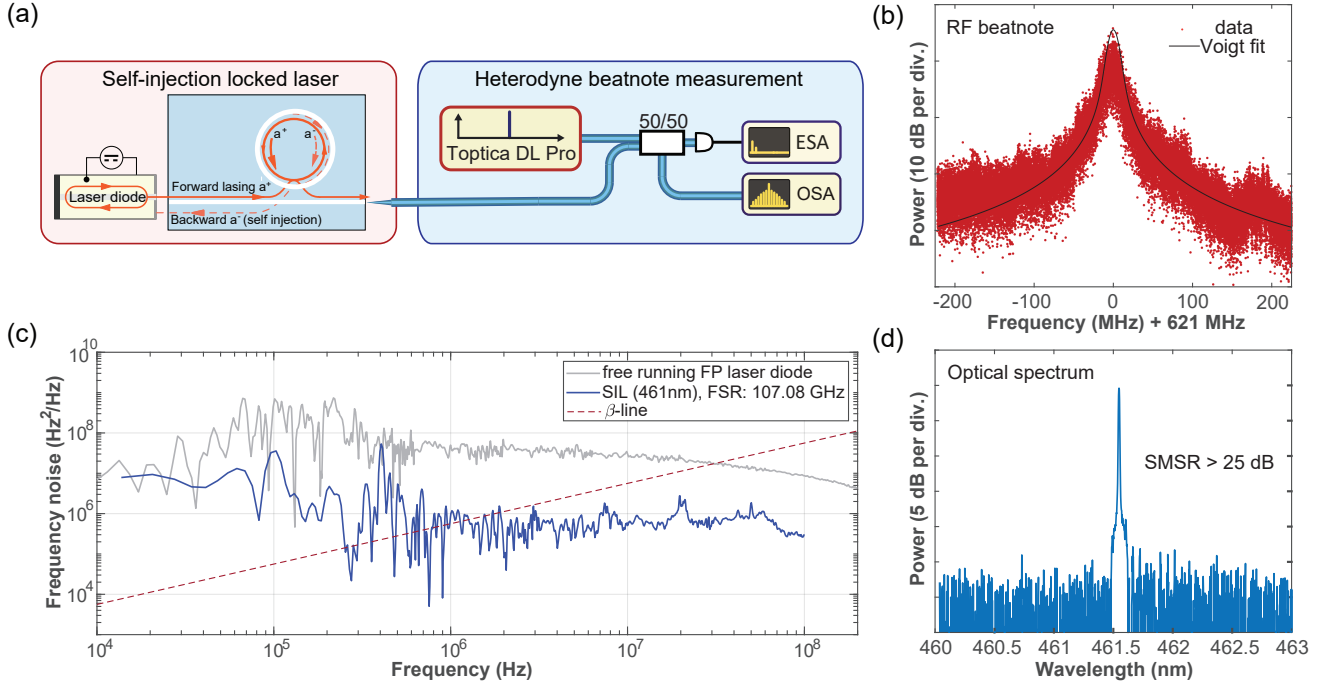


Figure 2. **III-N hybrid integrated laser performance characterization at 461 nm.** (a) Experimental scheme of laser frequency noise measurement using heterodyne beat with the reference laser (Toptica DL Pro) at 461 nm. (b) Heterodyne beat signal between the injection-locked laser and the reference laser. The measured beat signal is fitted with Voigt profile with Lorentzian FWHM ~ 2.7 MHz and Gaussian FWHM ~ 4.6 MHz. (c) Frequency noise spectra of the hybrid integrated laser system upon self-injection locking to microresonator with FSR 107.08 GHz. The grey line shows the frequency noise spectra of a free-running Fabry-Pérot laser diode. β -line is shown as reference (dashed line). (d) Optical spectrum of the self-injection locked Fabry-Pérot laser emission showing laser emission at 461.5 nm.

part is linked to the white noise and defines the intrinsic linewidth whereas the Gaussian part corresponds to the $1/f$ (flicker) and technical noise of the laser [32]. From fitting we extract a Lorentzian linewidth of ~ 2.7 MHz and a Gaussian linewidth of ~ 4.6 MHz. The specified linewidth of the reference laser is less than 500 kHz.

Figure 2c shows the frequency noise spectra of the free running Fabry Pérot laser and the self-injection locked laser. The frequency noise of the laser is determined via Welch's method [33] from a time sampling trace of the in-phase and quadrature components of the beatnote. The single sided phase noise power spectral density (PSD) $S_\phi(f)$ was converted to frequency noise $S_\nu(f)$ according to $S_\nu(f) = f^2 \cdot S_\phi(f)$. The self-injection locked laser optical spectrum is shown in Figure 2d indicating laser emission wavelength at 461.5 nm with side-mode suppression ratio of 25 dB. We also use the beta-line to quantify the linewidth of the self-injection locked laser by integrating the frequency noise spectra from the intersection of the PSD with the beta-line $S_\nu(f) = 8 \cdot \ln(2)f/\pi^2$ down to the integration time of the measurement. The integrated frequency noise A is used to evaluate the full-width half-maximum measure of the linewidth using $\text{FWHM} = \sqrt{8 \cdot \ln(2) \cdot A}$ [34]. We evaluate the FWHM as 3.72 MHz at 10 μ s integration time and 4.37 MHz at 0.1 ms integration time in agreement with the Voigt fit.

The laser self-injection locking suppresses the frequency noise by at least 10 dB across all frequency offsets.

Single-frequency lasing in near ultraviolet and visible regime. Next, we demonstrate self-injection locked laser in the near ultraviolet (410 nm), as well as in the green wavelength range using the same Si_3N_4 photonic chip as shown in Figure 3. Coupling the custom Al-GaInN near-UV laser diode for light emission at 410 nm (nominal output power of ca. 3.5 mW), we achieve laser self-injection locking at a diode current of 130 mA with fiber-coupled output power up to 0.15 mW. As shown in Figure 3, we achieve single-frequency lasing at 410.3 nm with side-mode suppression ratio greater than 18 dB. This constitutes the shortest wavelength hybrid integrated laser based on Si_3N_4 . The inset shows a photograph of the experimental setup where the laser diode is butt-coupled to the Si_3N_4 photonic chip. We clearly observe the scattering of near ultraviolet light around the circumference of the Si_3N_4 microresonator, which is indicative of the light inside the cavity. We also show operation in the visible. We attained single-frequency lasing at blue (461.8 nm) and green wavelengths (518.6 nm) via self-injection locking. The fiber-coupled output powers were 1 mW and 1.4 mW with side-mode suppression ratios of 24 dB and 28 dB respectively.

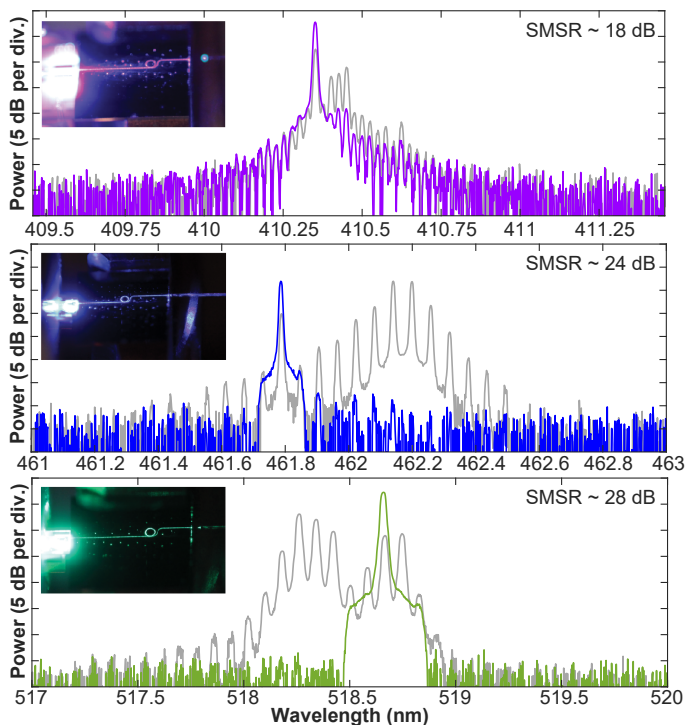


Figure 3. **III-N hybrid integrated laser based on self injection locking for several wavelengths from visible to near UV.** Optical spectra of self-injection locked laser states (single frequency) and multifrequency states (grey lines) at different wavelengths (near ultraviolet, blue and green) using the same Si_3N_4 photonic chip.

CONCLUSION

In conclusion, we have demonstrated a hybrid photonic integrated laser operating at near ultra-violet wavelengths as low as 410 nm for the first time. The custom AlGaInN-based laser gain elements were butt-coupled to a Si_3N_4 integrated photonic micro-ring resonator with high-Q for optical feedback and mode selection. For the photonic chip, we use Si_3N_4 photonic integrated circuits with a thickness of 50 nm and a uniform width of 600 nm

delivering a quality factor of $0.28 \cdot 10^6$ at a wavelength of 461.8 nm. The high quality factor of our near ultraviolet platform ensures single longitudinal mode lasing at green to near-ultraviolet wavelengths with linewidths as low as 2.7 MHz at 461.8 nm that are traditionally only achieved in bulk external cavity diode lasers. Further improvements of the device quality factor are possible by decreasing the Si_3N_4 waveguide core thickness, improving the waveguide roughness by using the photonic damascene reflow process [20, 35], and by improving the top oxide cladding [36], as well as by weakening confinement, which however comes at the cost of increasing the minimum bending ring radius and device footprint. We believe that by optimizing both the coupling between the laser-to-chip and chip-to-fiber and modest improvements of device quality factor, we can achieve multi-mW output powers and sub-100 kHz optical linewidths in the near-ultraviolet region, which would make our systems promising candidates for compact laser implementations for e.g. Sr^+ and Ca^+ atomic clocks.

Funding Information and Disclaimer: This material is based on research sponsored by Army Research Laboratory under agreement number W911NF-19-2-0345, by the Army Research Office under Cooperative Agreement number W911NF-20-2-0214, and by the Air Force Office of Scientific Research under award number FA9550-21-1-0063. This work was further supported by the Swiss National Science Foundation under grant agreement No. 176563 (BRIDGE) and by the European Space Technology Centre with ESA Contract No. 4000135357/21/NL/GLC/my. The U.S. Government is authorized to reproduce and distribute reprints for Government purposes notwithstanding any copyright notation thereon.

The views and conclusions contained herein are those of the authors and should not be interpreted as necessarily representing the official policies or endorsements, either expressed or implied, of Army Research Laboratory (ARL) or the U.S. Government.

Acknowledgments: The authors want to express their gratitude to Christopher Chua and Max Batres at PARC for their contributions in laser fabrication and characterization. We would also like to thank Arslan S. Raja, Jijun He and Snigrev Viacheslav for their assistance in experiments.

Data Availability Statement: The code and data used to produce the plots within this work will be released on the repository Zenodo upon publication of this preprint.

Correspondence and requests for materials should be addressed to T.J.K.

* johann.riemensberger@epfl.ch

† tobias.kippenberg@epfl.ch

- [1] A. Spott, E. J. Stanton, N. Volet, J. D. Peters, J. R. Meyer, and J. E. Bowers, Heterogeneous integration for mid-infrared silicon photonics, *IEEE Journal of Selected Topics in Quantum Electronics* **23**, 1 (2017).
- [2] W. Jin, Q.-F. Yang, L. Chang, B. Shen, H. Wang, M. A. Leal, L. Wu, M. Gao, A. Feshali, M. Paniccia, *et al.*, Hertz-linewidth semiconductor lasers using cmos-ready ultra-high-q microresonators, *Nature Photonics* **15**, 346 (2021).
- [3] B. Li, W. Jin, L. Wu, L. Chang, H. Wang, B. Shen, Z. Yuan, A. Feshali, M. Paniccia, K. J. Vahala, *et al.*,

Reaching fiber-laser coherence in integrated photonics, *Optics Letters* **46**, 5201 (2021).

- [4] G. Lihachev, J. Riemsensberger, W. Weng, J. Liu, H. Tian, A. Siddharth, V. Snigrev, R. N. Wang, J. He, S. A. Bhawe, *et al.*, Ultralow-noise frequency-agile photonic integrated lasers, *arXiv preprint arXiv:2104.02990* (2021).
- [5] G. Moody, V. J. Sorger, P. W. Juodawlkis, W. Loh, C. Sorace-Agaskar, M. Davanco, L. Chang, J. E. Bowers, N. Quack, C. Galland, *et al.*, Roadmap on integrated quantum photonics, *arXiv preprint arXiv:2102.03323* (2021).

- [6] R. J. Niffenegger, J. Stuart, C. Sorace-Agaskar, D. Kharas, S. Bramhavar, C. D. Bruzewicz, W. Loh, R. T. Maxson, R. McConnell, D. Reens, *et al.*, Integrated multi-wavelength control of an ion qubit, *Nature* **586**, 538 (2020).
- [7] A. D. Ludlow, M. M. Boyd, J. Ye, E. Peik, and P. O. Schmidt, Optical atomic clocks, *Reviews of Modern Physics* **87**, 637 (2015).
- [8] L. J. Mullen, A. J. Vieira, P. Herezfeld, and V. M. Con-tarino, Application of radar technology to aerial lidar systems for enhancement of shallow underwater target detection, *IEEE Transactions on microwave theory and techniques* **43**, 2370 (1995).
- [9] A. B. Ghisaidoobe and S. J. Chung, Intrinsic tryptophan fluorescence in the detection and analysis of proteins: a focus on förster resonance energy transfer techniques, *International journal of molecular sciences* **15**, 22518 (2014).
- [10] D. A. Kalashnikov, A. V. Paterova, S. P. Kulik, and L. A. Krivitsky, Infrared spectroscopy with visible light, *Nature Photonics* **10**, 98 (2016).
- [11] D. H. Card, D. L. Peterson, P. A. Matson, and J. D. Aber, Prediction of leaf chemistry by the use of visible and near infrared reflectance spectroscopy, *Remote Sensing of Environment* **26**, 123 (1988).
- [12] M. Chi, O. B. Jensen, A. K. Hansen, P. M. Petersen, and Y. Ma, Tunable high-power external-cavity gan diode laser systems in the visible spectral range, *Laser Technology and Its Applications*, 3 (2019).
- [13] P. S. Donvalkar, A. Savchenkov, and A. Matsko, Self-injection locked blue laser, *Journal of Optics* **20**, 045801 (2018).
- [14] D. Hofstetter, R. L. Thornton, L. T. Romano, D. P. Bour, M. Kneissl, and R. M. Donaldson, Room-temperature pulsed operation of an electrically injected ingan/gan multi-quantum well distributed feedback laser, *Applied physics letters* **73**, 2158 (1998).
- [15] S. Masui, K. Tsukayama, T. Yanamoto, T. Kozaki, S.-i. Nagahama, and T. Mukai, Cw operation of the first-order alingan 405 nm distributed feedback laser diodes, *Japanese journal of applied physics* **45**, L1223 (2006).
- [16] J. H. Kang, H. Wenzel, V. Hoffmann, E. Freier, L. Sulmoni, R.-S. Unger, S. Einfeldt, T. Wernicke, and M. Kneissl, Dfb laser diodes based on gan using 10th order laterally coupled surface gratings, *IEEE Photonics Technology Letters* **30**, 231 (2017).
- [17] T. J. Slight, S. Watson, S. Viola, A. Yadav, S. Stanczyk, S. Grzanka, S. Gwyn, E. Rafailov, P. Perlin, S. P. Najda, *et al.*, Recent progress in distributed feedback ingan/gan laser diodes, in *Novel In-Plane Semiconductor Lasers XVIII*, Vol. 10939 (International Society for Optics and Photonics, 2019) p. 109390I.
- [18] J. A. Holguin-Lerma, M. Kong, O. Alkhazragi, X. Sun, T. K. Ng, and B. S. Ooi, 480-nm distributed-feedback ingan laser diode for 10.5-gbit/s visible-light communication, *Optics letters* **45**, 742 (2020).
- [19] R. Jones, P. Doussiere, J. B. Driscoll, W. Lin, H. Yu, Y. Akulova, T. Komljenovic, and J. E. Bowers, Heterogeneously integrated inp/silicon photonics: fabricating fully functional transceivers, *IEEE Nanotechnology Magazine* **13**, 17 (2019).
- [20] J. Liu, G. Huang, R. N. Wang, J. He, A. S. Raja, T. Liu, N. J. Engelsens, and T. J. Kippenberg, High-yield, wafer-scale fabrication of ultralow-loss, dispersion-engineered silicon nitride photonic circuits, *Nature communications* **12**, 1 (2021).
- [21] M. C. Shin, A. Mohanty, K. Watson, G. R. Bhatt, C. T. Phare, S. A. Miller, M. Zadka, B. S. Lee, X. Ji, I. Datta, *et al.*, Chip-scale blue light phased array, *Optics letters* **45**, 1934 (2020).
- [22] T. Pan, D. Lu, H. Xin, and B. Li, Biophotonic probes for bio-detection and imaging, *Light: Science & Applications* **10**, 1 (2021).
- [23] G. Liang, H. Huang, A. Mohanty, M. C. Shin, X. Ji, M. J. Carter, S. Shrestha, M. Lipson, and N. Yu, Robust, efficient, micrometre-scale phase modulators at visible wavelengths, *Nature Photonics*, 1 (2021).
- [24] M. Corato-Zanarella, A. Gil-Molina, X. Ji, M. C. Shin, A. Mohanty, and M. Lipson, Widely tunable and narrow linewidth chip-scale lasers from deep visible to near-ir, *arXiv preprint arXiv:2109.08337* (2021).
- [25] E. Feltin, A. Castiglia, G. Cosendey, L. Sulmoni, J.-F. Carlin, N. Grandjean, M. Rossetti, J. Dorsaz, V. Laino, M. Duell, *et al.*, Broadband blue superluminescent light-emitting diodes based on gan, *Applied Physics Letters* **95**, 081107 (2009).
- [26] K. Luke, A. Dutt, C. B. Poitras, and M. Lipson, Overcoming si 3 n 4 film stress limitations for high quality factor ring resonators, *Optics express* **21**, 22829 (2013).
- [27] T. J. Morin, L. Chang, W. Jin, C. Li, J. Guo, H. Park, M. A. Tran, T. Komljenovic, and J. E. Bowers, Cmos-foundry-based blue and violet photonics, *Optica* **8**, 755 (2021).
- [28] Y. Lin, J. C. Mak, H. Chen, X. Mu, A. Stalmashonak, Y. Jung, X. Luo, P. G.-Q. Lo, W. D. Sacher, and J. K. Poon, Low-loss broadband bi-layer edge couplers for visible light, *Optics Express* **29**, 34565 (2021).
- [29] V. Vassiliev, V. Velichansky, P. Kersten, and F. Riehie, Injection locking of a red extended-cavity diode laser, *Electronics Letters* **33**, 1222 (1997).
- [30] A. S. Raja, A. S. Voloshin, H. Guo, S. E. Agafonova, J. Liu, A. S. Gorodnitskiy, M. Karpov, N. G. Pavlov, E. Lucas, R. R. Galiev, *et al.*, Electrically pumped photonic integrated soliton microcomb, *Nature communications* **10**, 1 (2019).
- [31] A. A. Savchenkov, S.-W. Chiow, M. Ghasemkhani, S. Williams, N. Yu, R. C. Stirbl, and A. B. Matsko, Self-injection locking efficiency of a uv fabry-perot laser diode, *Optics letters* **44**, 4175 (2019).
- [32] G. Stéphan, T. Tam, S. Blin, P. Besnard, and M. Têtu, Laser line shape and spectral density of frequency noise, *Physical Review A* **71**, 043809 (2005).
- [33] P. Welch, The use of fast fourier transform for the estimation of power spectra: a method based on time averaging over short, modified periodograms, *IEEE Transactions on audio and electroacoustics* **15**, 70 (1967).
- [34] G. Di Domenico, S. Schilt, and P. Thomann, Simple approach to the relation between laser frequency noise and laser line shape, *Applied optics* **49**, 4801 (2010).
- [35] M. H. Pfeiffer, J. Liu, A. S. Raja, T. Morais, B. Ghadiani, and T. J. Kippenberg, Ultra-smooth silicon nitride waveguides based on the damascene reflow process: fabrication and loss origins, *Optica* **5**, 884 (2018).
- [36] J. F. Bauters, M. J. Heck, D. D. John, J. S. Barton, C. M. Bruinink, A. Leinse, R. G. Heideman, D. J. Blumenthal, and J. E. Bowers, Planar waveguides with less than 0.1 db/m propagation loss fabricated with wafer bonding, *Optics express* **19**, 24090 (2011).